Available online at www.sciencedirect.com
SCIENCE DIRECT®
Coordination Chemistry Reviews 247 (2003) 1–19
COORDINATION CHEMISTRY REVIEWS
www.elsevier.com/locate/ccr

Review

Developments in the metal chemistry of N-confused porphyrin

John D. Harvey, Christopher J. Ziegler*

[a] *Department of Chemistry, Buchtel College of Arts and Sciences, University of Akron, Akron, OH 44325-3601, USA*

Received 18 February 2003; accepted 23 July 2003

Contents

Abstract

Since its discovery as a side product in acid catalyzed condensations in 1994, the metal chemistry of N-confused porphyrins has grown exponentially. Due to the location of an external nitrogen on the porphyrin skeleton, different binding modes are being discovered for N-confused porphyrin as compared to tetraphenylporphyrin. In this paper, the metal chemistry of N-confused porphyrin is discussed, reviewing coordination modes and literature on the metal complexes to date.
© 2003 Elsevier B.V. All rights reserved.

Keywords: N-confused porphyrin; 2-Aza-21 carbaporphyrin; Inverted porphyrin; Metalloporphyrin

1. Introduction

1.1. Background

In coordination chemistry, few ligands have been as heavily studied as the porphyrin macrocycle [1]. The metal complexes of both synthetic and natural porphyrins have been explored across the periodic table, and nearly all of the elements have been complexed to this macrocycle [2]. This work has lead to compounds that have relevance to biological systems [3], can be used as catalysts for organic transformations [4], and are promising candidates for advanced materials components [5]. Despite the apparently exhaustive investigation of the metal chemistry of porphyrin over the latter part of the last century, the field remains active and many metalloporphyrin publications continue to appear in the literature [6–8].

While the transition and main group chemistry of normal porphyrins are relatively well understood [2], the metallation chemistry of related tetrapyrrolic macrocycles is still largely unexplored. Recent reports in the organic literature have presented the syntheses and characterization of new aromatic tetrapyrroles, and the past few years have demonstrated significant advancements in the development of one step, high yield preparations for many of these compounds [9,10]. These aromatic tetrapyrroles include the isomers of porphyrin, where the $C_{20}N_4$ skeleton of the macrocycle is rearranged, and the analogs of porphyrin, where the skeleton is expanded, contracted, or the nitrogens replaced with other elements. The isomers of porphyrin (Fig. 1a) include macrocycles, such as porphycene, hemiporphycene, and corphycene (Fig. 1b–d) [11] where the meso carbons are rearranged to form new macrocycle structures. The analogs of porphyrin are more diverse, and range from contracted

* Corresponding author. Tel.: +1-330-972-2531; fax: +1-330-972-7370.
E-mail address: ziegler@uakron.edu (C.J. Ziegler).

0010-8545/$ – see front matter © 2003 Elsevier B.V. All rights reserved.
doi:10.1016/j.cct.2003.07.001

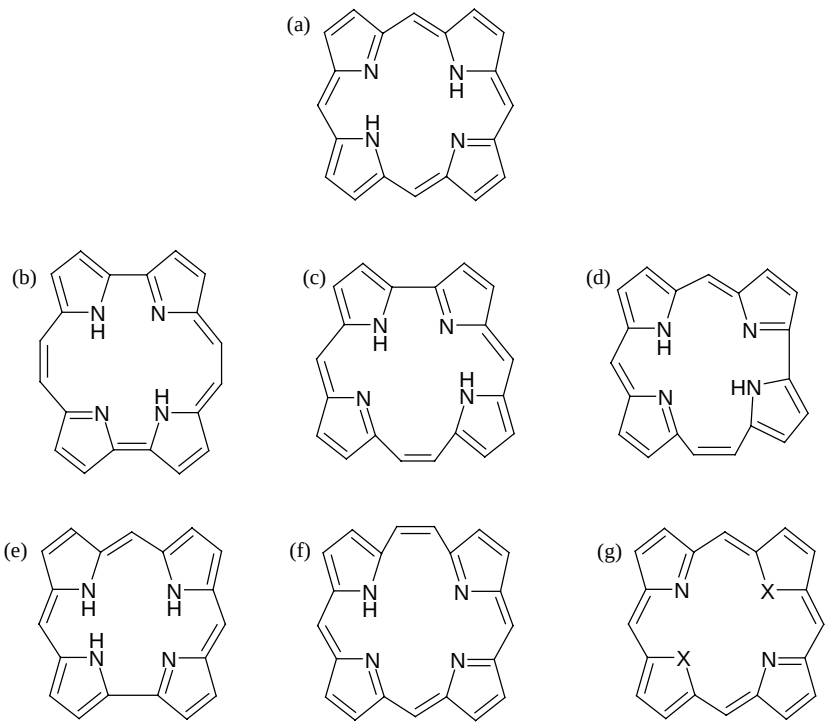

Fig. 1. The structures of tetrapyrrolic porphyrin isomers and analogs: porphyrin (a), porphycene (b), hemiporphycene (c), and corrphycene (d), corrole (e), homophyrins (f), thiaporphyrins (g, X = S), and oxaporphyrins (g, X = O) [11–27].

macrocycles, such as corrole (Fig. 1e) [12–19], to expanded systems like the homophyrins (Fig. 1f) [20], and heteroatom substituted macrocycles, such as thiaporphyrins [21–24] and oxaporphyrins [25–27] (Fig. 1g).

This review will examine the metal chemistry of a relatively new isomer of porphyrin, 2-aza-21-carbaporphyrin, also known as inverted porphyrin or N-confused porphyrin [28,29]. As can be seen in Fig. 2, N-confused porphyrin is very similar to the parent porphyrin macrocycle, but has a carbon atom occupying one of the interior pyrrolic positions, and a nitrogen at a normally β-pyrrolic site on the periphery of the ring. In addition to the singly N-confused porphyrin, a doubly confused variant has also been synthesized through condensation of two confused dipyrromethanes with pentafluorobenzaldehyde [30].

Singly N-confused porphyrin was first isolated as a byproduct of normal acid catalyzed condensations of

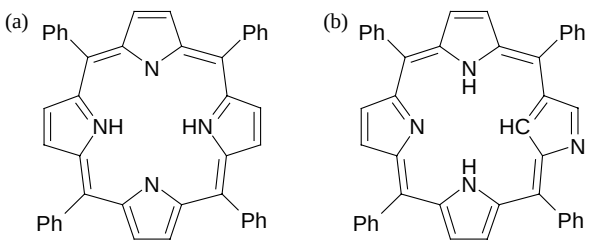

Fig. 2. The structures of freebase tetraphenylporphyrin (a), and the internally protonated freebase N-confused tetraphenylporphyrin (b) [28,29].

pyrrole and benzaldehyde [28,29]. Not surprisingly, the yields of confused porphyrin from these reactions were extremely low. The first confused porphyrin rings reported were 5,10,15,20-tetraphenyl-2-aza-21-carbon porphyrin, or N-confused tetraphenylporphyrin (H_2NCTPP) and 5,10,15,20-tetratolyl-2-aza-21-carbon porphyrin (CTTPH_2). Papers on the preparation of these macrocycles were published simultaneously by two groups in 1994; one group led by Lechoslaw Latos-Grażyński [29] and a second by Hiroyuki Furuta [28]. Furuta synthesized H_2NCTPP by the reaction of pyrrole and benzaldehyde in a solution of *tert*-BuOH/CH_2Cl_2 and HBr (Fig. 3a). The solution is then oxidized by chloranil, purified by column chromatography and crystallized using CH_2Cl_2/MeOH. NCTPP is obtained in yields of 5–7% with the major product still being tetraphenylporphyrin, H_2TPP. At about the same time that Furuta and co-workers published their results on H_2NCTPP, Lechoslaw Latos-Grażyński published results on another confused porphyrin derivative [29]. Latos-Grażyński synthesized the confused porphyrin CTTPH_2 using *p*-tolylaldehyde with pyrrole in CH_2Cl_2 with $BF_3{\cdot}Et_2O$ as the catalyst for the reaction (Fig. 3b). CTTPH_2 is identical to H_2NCTPP, but CTTPH_2 has four tolyl groups at the meso carbons.

Initially, the limited yields of these two reactions prevented the widespread investigation of the metal chemistry of N-confused porphyrin. In 1999, Lindsey and co-workers published an improved synthesis of H_2NCTPP (Fig. 3c) [31]. H_2NCTPP can be produced by addition of

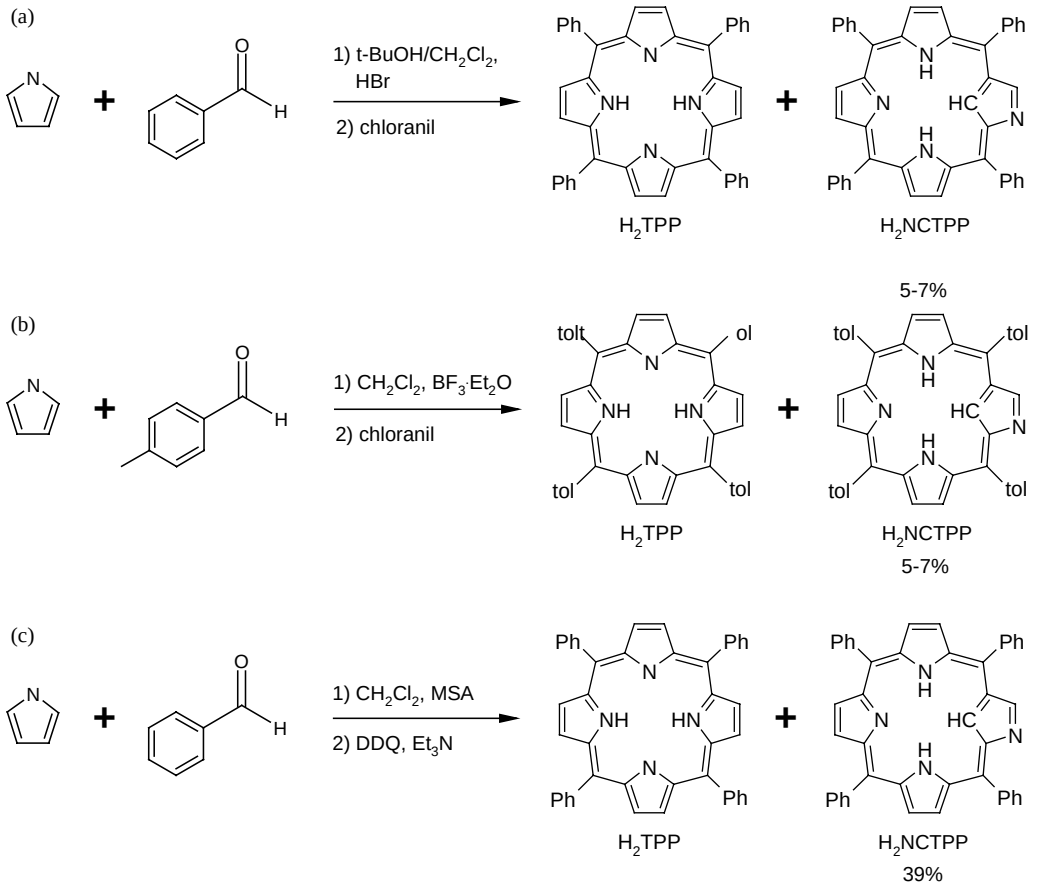

Fig. 3. Synthetic procedures for generation of H_2NCTPP: Furuta et al. (a) Latos-Grażyński et al. (b) Lindsey et al. (c) [28,29,31].

methanesulfonic acid to a solution of CH_2Cl_2 containing equal moles of pyrrole and benzaldehyde. The solution is stirred for 30 min, and then the reaction is oxidized by DDQ followed by acid quenching with triethylamine. Subsequent column chromatography with alumina yields 39% H_2NCTPP, and the reaction can be readily scaled up to afford gram-scale quantities of the macrocycle.

The exact mechanism of formation of N-confused porphyrin is not yet elucidated, but it was postulated by Latos-Grażyński and co-workers that two different conformations of tetrapyrromethane are present before ring closure [30]. Ring closures at the α or β position are both possible, depending on the orientation of the tetrapyrromethane. Furuta proposed that anion templating could play a role in N-confused porphyrin formation because H_2NCTPP was generated in the presence of Cl^- and Br^-, but not in the presence of F^-, TFA^-, NO_3^-, or $H_2PO_4^-$ [29]. A survey done by Lindsey on the acid catalysts used for the formation of porphyrinic macrocycles showed that sulfonic acids give H_2NCTPP in the highest yields, but why certain acids support N-confused porphyrin formation was not proposed [32].

The ready availability of N-confused porphyrins has initiated an explosive growth in the preparation and isolation of transition and main group metal complexes. Since the appearance of the improved synthesis by Lindsey et al., the number of N-confused porphyrin metal complexes presented in the literature has quadrupled. This review will present the current state of research in the coordination chemistry of N-confused porphyrins. Even at this early stage, it is clear N-confused metalloporphyrins adopt widely diverse geometries, and that the simple inversion of two atoms in the porphyrin skeleton has a significant effect on the structure and reactivity of this macrocycle and its derivatives.

1.2. N-confused porphyrin as a ligand

Upon examination of N-confused porphyrin, it is clear that this macrocycle could adopt several structures when coordinated to metals due to the presence of the external nitrogen. These questions prompted studies into the acid-base chemistry of N-confused porphyrin to probe the Lewis basicity of the inverted pyrrole. Both Furuta and Latos-Grażyński demonstrated that the interior and exterior nitrogen sites in N-confused porphyrin could be protonated. Furuta and coworkers used an excess (1000 equivalents) of trifluoroacetic acid to protonate these sites in H_2NCTPP [28]. The Soret band in the UV-Vis absorption spectrum shifted from 438 to 451 and 465 nm, and Q bands also red shifted from 725 to 800 and 825 nm for the monoprotonated and diprotonated forms, respectively. Latos-Grażyński

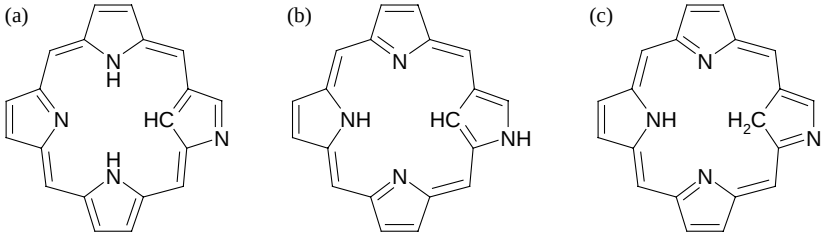

Fig. 4. Proposed tautomers of freebase N-confused porphyrin: internally protonated (a), externally protonated (b), and internal carbon doubly protonated (c) [36].

independently confirmed the protonation of this macrocycle using deuterated acetic acid, and was able to deuterate both the 21 position as well as the interior pyrrolic site [29]. The identities of the sites of protonation were confirmed by using 2D ^{1}H COSY and NOESY NMR experiments.

With the knowledge that different forms of protonation in H_2NCTPP were possible, it was possible to propose the existence of multiple tautomers for N-confused porphyrin. In normal porphyrins, the tautomerization of the inner pyrrolic protonation sites occurs rapidly and does not affect how porphyrin acts as a ligand for metal complexation. Initial theoretical work on N-confused porphyrins by Szterenberg and Latos-Grażyński [33], Ghosh et al. [34], and later by Furuta [35] proposed the existence of three tautomers, shown in Fig. 4. These initial calculations found that the interior protonated form, tautomer 4a, is the most stable form. However, these studies concluded that the difference in energies between form 4a and the externally protonated tautomer, 4b, is surprisingly small (∼3.4–5.7 kcal/mol). This small difference lead to the conclusion that the tautomers 4a and 4b might both be isolated. The third tautomer 4c, where the internal carbon in doubly protonated, is more destabilized relative to 4a (an average of 5.8 kcal/mol over three calculations by Szterenberg and Latos-Grażyński) [33], but is relevant to the some of the more recently elucidated metal binding geometries.

The original synthesis of N-confused porphyrins resulted in the isolation of the internally protonated tautomer, 4a, from non-polar solvents [28]. Several years later, Furuta et al. isolated the externally protonated tautomer of H_2NCTPP (4b) by varying solvent conditions [36]. Absorption spectra for H_2NCTPP display striking differences compared to H_2TPP and are highly solvent dependent [36]. As can be seen in Fig. 5, each tautomer has distinctive absorption characteristics. In non-polar media, H_2NCTPP forms a red solution, but in polar solvents this macrocycle is green in color. In a polar solvent, such as dimethylacetamide (DMAc), the externally protonated form is more stable, presumably because of either hydrogen-bonding or dipole–dipole interactions of the exocyclic N–H bond with solvent, whereas a less polar solvent, such as $CHCl_3$ tends to favor the internally protonated form. In DMAc, the Soret band for H_2NCTPP (4b) is significantly red-shifted (441 nm) relative to the Soret band of H_2TPP (419 nm). Three Q-band absorptions of increasing intensity are found at 695, 642, and 592 nm, along with a smaller shoulder at 550 nm. Similar to the red-shift in the Soret band, these bands are 37–50 nm lower in energy than the corresponding absorptions in H_2TPP. Unlike H_2TPP, however, the intensities of these bands increase slightly with decreasing energy, with the lowest-energy absorption being most intense. A high-energy band occurring at 381 nm can be attributed to N-band absorption.

In $CHCl_3$, the Soret band for the internally protonated form (4a) is similarly red-shifted (438 nm). Three pronounced Q-band absorptions are observed in $CHCl_3$ at 539, 580, and 724 nm, with two smaller absorptions at 504 and

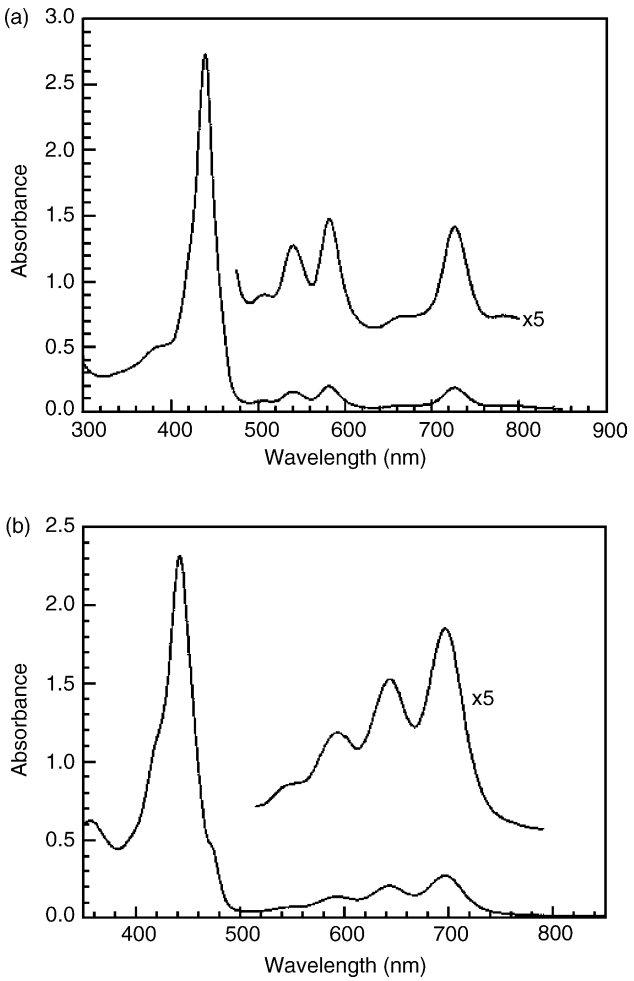

Fig. 5. Visible absorption spectra of internally protonated (a) and externally protonated (b) tautomers of H_2NCTPP [37].

665 nm. An increase in the intensities of the Q-band absorptions is also observed in this tautomer that corresponds with a decrease in the absorption band energy. Two weak absorptions are observed at 353 and 504 nm, with the former being attributed to the N band. The intensity profile of Q-band region, particularly that of the low energy absorption at 724 nm for the internal tautomer, is reminiscent of the absorption spectra of reduced porphyrins (i.e. hydrogenated at one of the pyrrole rings), such as chlorins and chlorophylls *a* and *b*.

Further characterization of the two tautomers of H_2NCTPP was obtained by ^{1}H NMR in $CDCl_3$ and DMF-d_7 [36]. In $CDCl_3$, two peaks are observed at −4.99 and −2.41 ppm. The peak at −2.41 ppm is split into a doublet, indicating two interior NH groups while the peak at −4.99 ppm is a singlet arising from the inner CH. When ^{1}H NMR was carried out using DMF-d_7, all signals relating to interior protons (at 0.76 and 2.27 ppm) are singlets and a new signal at 13.54 ppm appears. This deshielded signal was assigned to the external nitrogen being protonated, and was further confirmed through examination of the ^{15}N NMR of ^{15}N labeled H_2NCTPP. In the externally protonated tautomer (4b), the 18-electron annulene ring is abrogated due to the lack of conjugation through the external nitrogen. This reduction in aromaticity in 4b also helps to explain the upfield shift of the interior proton relative to that of the internally protonated tautomer.

Structural data on the two tautomers were obtained by X-ray crystallography. Two crystal structures of H_2NCTPP grown from CH_2Cl_2/MeOH and DMF/MeOH display the structures of the interior and exterior protonated tautomers, respectively, in the solid state [28,36]. As stated above, tautomer 4a has three interior protons and the confused pyrrole is canted out of the interior nitrogen plane by 26.9° (Fig. 6a). Tautomer 4b (Fig. 6b) is considerably more planar with the pyrrole rings tilted by only 4.7, 0.2, 2.8, and 0.9°. When the external nitrogen proton is absent, the three interior protons have enough steric bulk to repel one another and deform the confused pyrrole out of the plane of the macrocycle. If the external nitrogen is protonated, only two protons are present in the interior. This allows for the formation of a more planar macrocycle, similar to H_2TPP.

In our group, we have reexamined the electronic structures of both tautomers using DFT methods at the B3LYP/6-31G(d)//B3LYP/3-21G(d) level using the observed crystal structures as a starting point for the geometry optimization [37]. We also carried out these calculations in the context of Gouterman's four orbital model (HOMO-1, HOMO, LUMO, LUMO+1), which provides some insight into how these macrocycles can function as ligands for metals [38,39]. Plots of the four frontier orbitals are shown in Fig. 7 compared to those of tetraphenylporphyrin, H_2TPP. Our calculated energies are in agreement with the previously determined calculations by Szterenberg and Latos-Grażyński [33] and Ghosh et al. [34]. As can be seen in the four orbital MO diagrams, the electronic structures

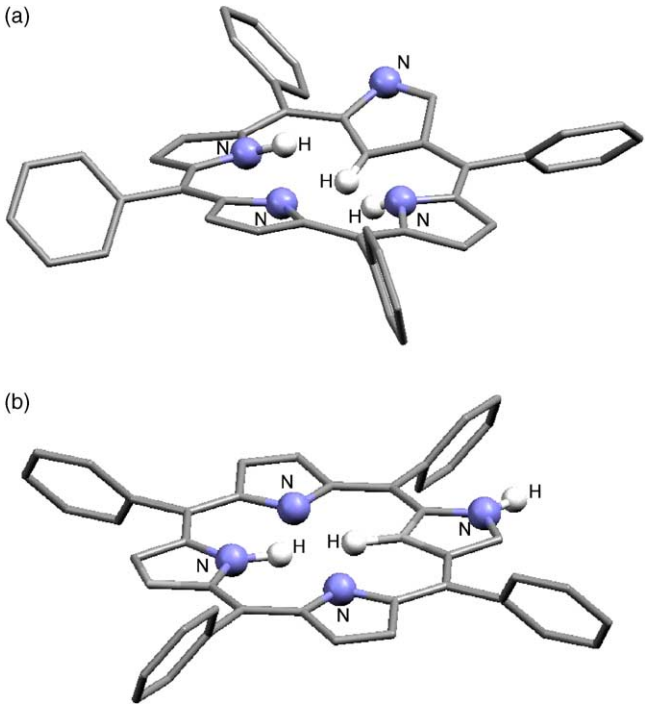

Fig. 6. Crystal structures of the internally protonated (a) and externally protonated (b) tautomers of H_2NCTPP [28,36].

of each tautomer are quite different, as observed in the absorption spectrum of each. The four orbitals of the internally protonated tautomer (4a) resemble more closely those of normal tetraphenylporphyrin, while those of the other tautomer have much less symmetry at the confused pyrrole ring.

In addition to the changes in electronic structure between the two tautomers, the changes in protonation within the core indicate that N-confused porphyrins can have variable charge. Complete deprotonation of the 4a tautomer will result in a trianionic ligand similar to that observed in corrole [40]. This increased charge relative to normal porphyrins indicates that this macrocycle may stabilize high oxidation states in metals. Alternatively, the externally protonated tautomer will only have a dianionic charge if both protons in the pore are removed and will behave in a fashion similar to a normal porphyrin. This variable deprotonation in N-confused porphyrins is complicated by the lack of acidity of the internal carbon. As will be shown below, some metal complexes retain the internal C–H bond. This factor, plus the basic character of the external nitrogen, can result in some ambiguity over the charge of the macrocycle or metal oxidation state in resultant complexes.

2. Metal complexes of NCTPP

2.1. Monomeric complexes

The first metal complex of an N-confused porphyrin was presented along with the synthesis of the macrocycle [29].

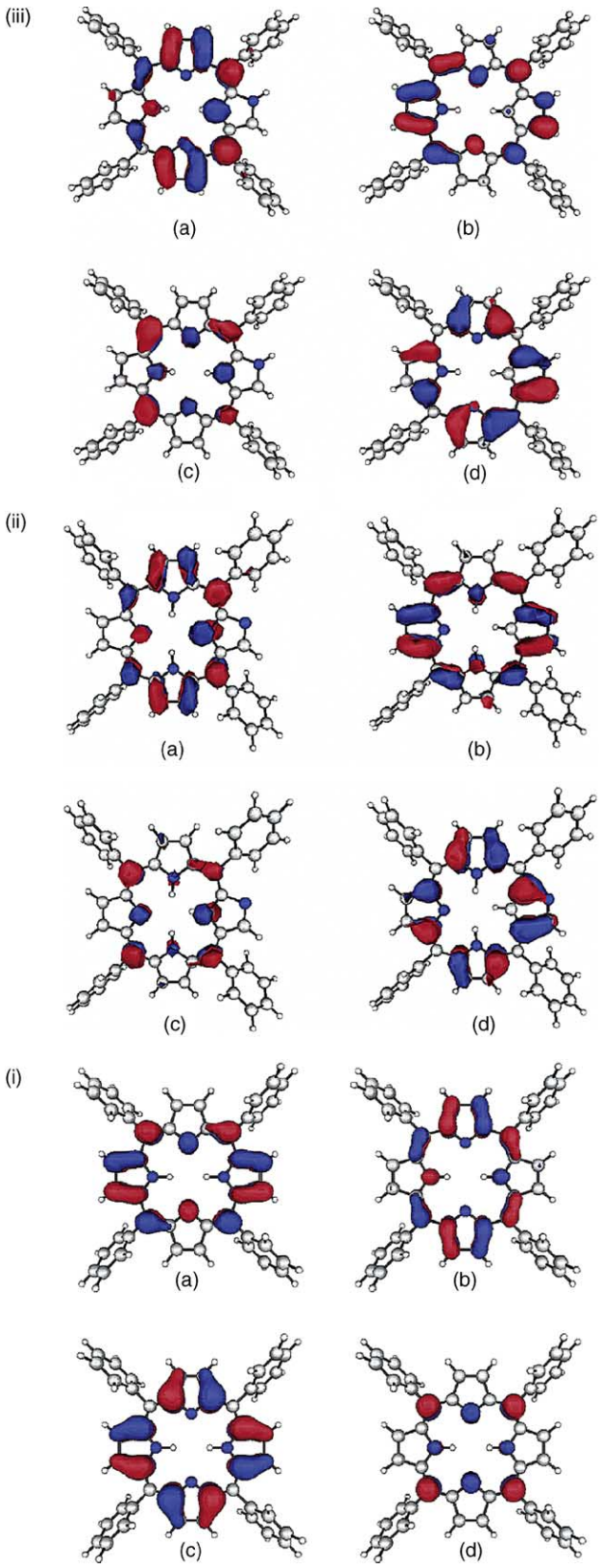

Fig. 7. Plots of the LUMO+1 (a), LUMO (b), HOMO (c), and HOMO-1 (d) molecular orbitals for H_2TPP (i), internally protonated H_2NCTPP (ii), and externally protonated H_2NCTPP (iii). These orbitals were calculated at the B3LYP/6-31G (d) level [37].

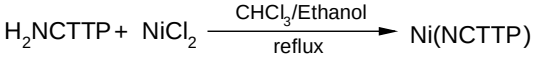

Scheme 1.

Latos-Grażyński et al. inserted nickel into H_2NCTTP by refluxing an ethanol solution containing $NiCl_2$ with a $CHCl_3$ solution of the macrocycle (Scheme 1). Subsequent purification by silica gel chromatography yields Ni(NCTTP) in 40% yield. The structure of this compound was elucidated by single crystal X-ray diffraction and is shown in Fig. 8. The structure shows that the nickel lies in the plane of the macrocycle and that the ring itself is largely planar. Deprotonation and subsequent coordination of the interior carbon along with protonation of the external nitrogen were observed by disappearance of the interior proton signal near −5.0 ppm and appearance of a proton resonance at 10.2 ppm, respectively. In addition, Ni(NCTTP) is a diamagnetic species, and therefore, NCTTP in this case acts as a dianionic ligand, stabilizing Ni(II). The Soret band of Ni(NCTTP) is at 426 nm, which is significantly blue shifted from the Soret bands of either tautomer, which appear at 438 and 441 for the internal and external tautomers, respectively. This increase in the energy of the π–π^* transition is analogous to that found in Ni(TPP), which is characterized as a hypso porphyrin [41]. The Q-band structure is significantly perturbed from either form of the free base, however [28,29,36].

Soon after the presentation of the nickel derivative, Chmielewski and Latos-Grażyński were able to methylate the interior pyrrolic CH of Ni(NCTPP) by using methyl iodide [42]. Reaction of Ni(NCTPP) with an excess of CH_3I in CH_2Cl_2 results in the formation of three Ni(NCTPP) derivatives in the same reaction flask; the interior methylated form, Ni(21-CH_3NCTPP), the internal methylated form with an axial halide, Ni(21-CH_3NCTPP)X, and an internal and external methylated form with an axial halide, Ni(2-$NCH_3$21–CH_3NCTPP)X. The three products were

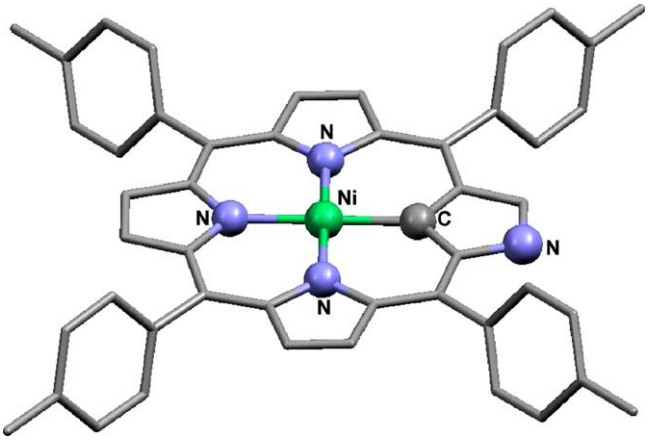

Fig. 8. Crystal structure of Ni(NCTTP); due to disorder resulting from the high symmetry in the structure, the confused pyrrole assignment is ambiguous and one of eight possible orientations is shown [29].

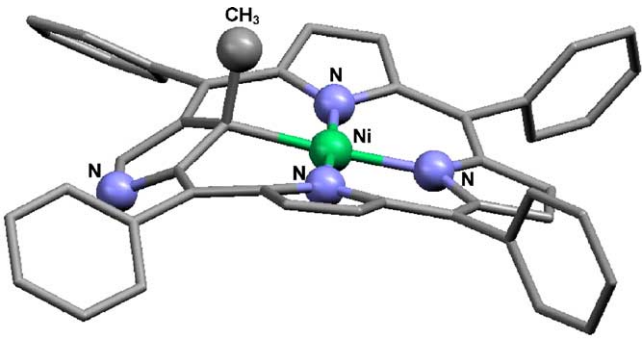

Fig. 9. Crystal structure of Ni(C21–CH_3–NCTPP) [42].

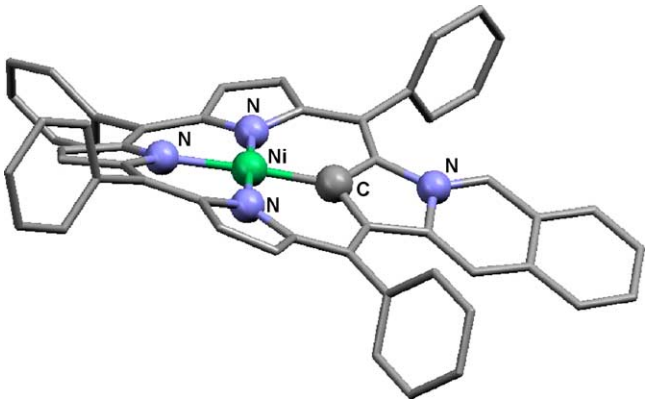

Fig. 11. Crystal structure of Ni(N-confused isoquinone porphyrin) [45].

then separated by using column chromatography, and the iodide was exchanged for chloride by washing with 5% aqueous HCl. Ni(21-CH_3NCTPP) exhibits a spectrum with a blue shifted Soret at 430 nm with poorly defined Q bands at 550, 610, and 735 nm. The second form, Ni(21-CH_3NCTPP)Cl has a red shifted Soret at 445 nm, with better defined Q bands structure at 580, 730, and 820 nm. The doubly methylated form, Ni(2-$NCH_3$21–CH_3NCTPP)X has an even further red shifted Soret at 465 nm with a significant decrease in intensity relative to the two monomethylated forms. The Q band structure is unchanged from Ni(21-CH_3NCTPP)Cl, with Q bands of 465, 580, 730, and 820 nm. Isolation of the externally methylated Ni(2-NCH_3NCTPP) complex was carried out by first methylating the porphyrin ring and then reacting with nickel acetate [43]. Purification of this product results in isolation of a material with a Soret at 430 nm and Q-bands of 464, 563, 660, 712, and 776 nm. The authors state that the axially coordinated complexes are paramagnetic upon observation of the isotropic shifts of the pyrrole and phenyl resonances in the ^{1}H NMR spectrum.

X-ray crystallography of Ni(21-CH_3NCTPP) reveals the structure of the complex (Fig. 9) [42]. The three Ni–N bond lengths are similar to those observed for four coordinate nickel porphyrin complexes, but the Ni–C bond (2.005 Å) is slightly longer than that found in Ni(NCTTP) (1.963 Å). Both the nickel (0.097 Å) and internal CH_3 group (0.074 Å) rise above the plane of the macrocycle in the same direction. The porphyrin ring is not planar, and the confused pyrrole is tilted (42.2°) toward the opposite side of the ring away from the metal while the other three pyrroles are tilted in the opposite direction from the metal. Structural characterization of Ni(2-$NCH_3$21–CH_3NCTPP)I (Fig. 10) shows similar structural features to those of Ni(21-CH_3NCTPP) [42]. All the pyrroles are tilted in a similar fashion (55.3° for the confused pyrrole) and the internal methyl is also above the macrocycle. This structure has the nickel on the side of the porphyrin ring opposite the internal methyl group, coordinated by an iodide. The Ni–N bonds are longer, being more similar to six coordinate nickel compounds rather than those of Ni(21-CH_3NCTPP).

Protonation of the internal carbon has been observed for Ni(NCTPP) and Ni(2-NCH_3NCTPP) [44]. Characterization by ^{1}H NMR at 233 K reveals a new proton resonances at −3.10 ppm, similar to the zinc adduct as will be discussed later. ^{13}C NMR resonances show that the internal carbon is sp^3 hybridized and must coordinate in a $^1\eta$ mode to the nickel center. This is particularly relevant to several transition metal structures where the internal C–H bond remains intact upon metallation.

David Dolphin and coworkers were able to use Ni(NCTPP) as a dienophile in a Diels–Alder reaction [45]. Reaction of Ni(NCTPP) with sultine in refluxing benzene for 2 days followed by purification of the reaction by chromatography yields a nickel N-confused isoquinone porphyrin. The absorption spectrum of this complex has a Soret band at 438 nm and a Q band at 628 nm. Explicit structural determination was completed by X-ray crystallographic analysis (Fig. 11). The isoquinone is linked to and lies in

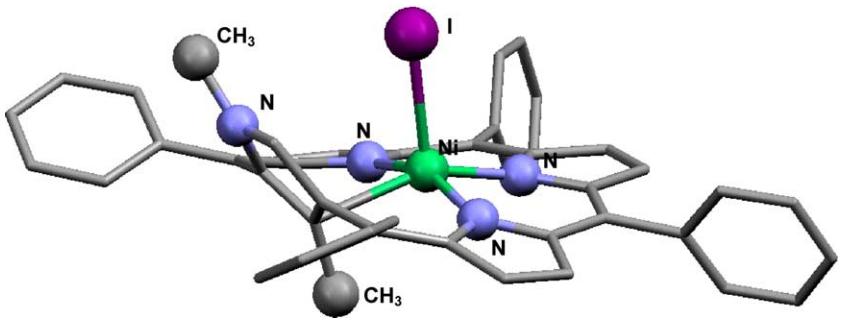

Fig. 10. Crystal structure of Ni(N2–CH_3–C21–CH_3–NCTPP)I [42].

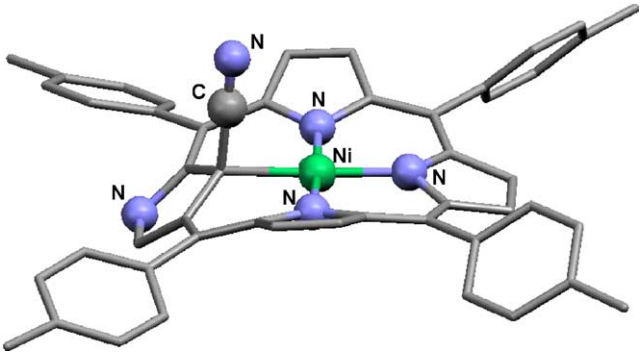

Fig. 12. Crystal structure of Ni((C–CN)NCTTP) [46].

the same plane as the confused pyrrole. Unlike Ni(NCTPP), the porphyrin macrocycle is ruffled which results in shorter nitrogen bond lengths to nickel.

Continuing his work with Ni(NCTTP), Dolphin and coworkers reacted Ni(NCTTP) with sodium methoxide in the presence of an oxidant, DDQ, which generated two Ni(NCTTP) products [46]. One product has a cyanide group bound to the internal carbon. NMR of this complex exhibits a signal at 10.03 ppm for the external CH on the confused pyrrole, which is shifted 1.5 ppm further downfield compared to other β protons. Since the internal carbon is nearly sp^3 hybridized, the author states that this shift supports π delocalization through the outer pathway of the confused pyrrole because conjugation of the internal carbon would not be possible. The second product also has cyanide at the internal carbon and a methoxide added at the β carbon next to the external nitrogen. Structural determination of both products by X-ray crystallography is shown in Fig. 12 and Fig. 13. The tilting of the pyrrole rings is similar to the tilts observed in the internally methylated Ni(NCTTP).

To examine whether H_2NCTPP could stabilize metals in higher oxidation states, Furuta et al. reacted this macrocycle with silver triflouroacetate in CH_2Cl_2/MeOH (Scheme 2)

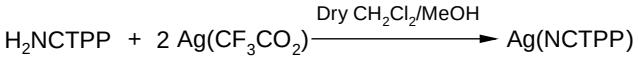

Scheme 2.

[47]. The structure of the resulting Ag complex (characterized by X-ray crystallography) shows the metal to be in a nearly square planar geometry in the plane of the macrocycle (Fig. 14). The external nitrogen is not protonated in this case, resulting in a trianionic ligand and an oxidation state assignment of 3+ for the metal. The oxidation state of silver in this complex was confirmed by magnetic susceptibility measurements, lack of counter anions in the crystalline lattice, and NMR spectroscopy. The absorption spectrum in CH_2Cl_2 displays a red shifted Soret band at 447.5 nm and four Q-bands at 520, 554, 588, and 637 nm, respectively. This spectrum resembles that of the internally protonated free base tautomer (539, 580, 665, 724 nm), although it is blue shifted significantly.

Soon after the appearance of the silver product, Chmielewski et al. presented the copper derivative isolated by mixing copper acetate with H_2NCTPP in THF under anaerobic conditions [44]. Removal of the solvent, and extraction of the product with toluene followed by addition of hexane afforded a brown precipitate. Absorption spectrum of the product in CH_2Cl_2 showed a change in the absorption characteristics relative to free base, with features at 331, 388, 432sh, 451, 542, 588sh, 680, and 739 m. The EPR of the product shows a signal with a hyperfine contribution for a Cu(II) center and the presence of superhyperfine patterns corresponding to the three nitrogens in the NCTPP core. Electrospray mass spectrometry characterization exhibits a product peak at 676 M/z, which corresponds to a $[M + 1]^+$ for Cu(NCTPP). The mass spectrum, however, does not indicate if the external nitrogen is protonated or if the internal pyrrolic carbon is deprotonated. Treatment of the product with TFA/HCl in CH_2Cl_2 provides a new spectrum,

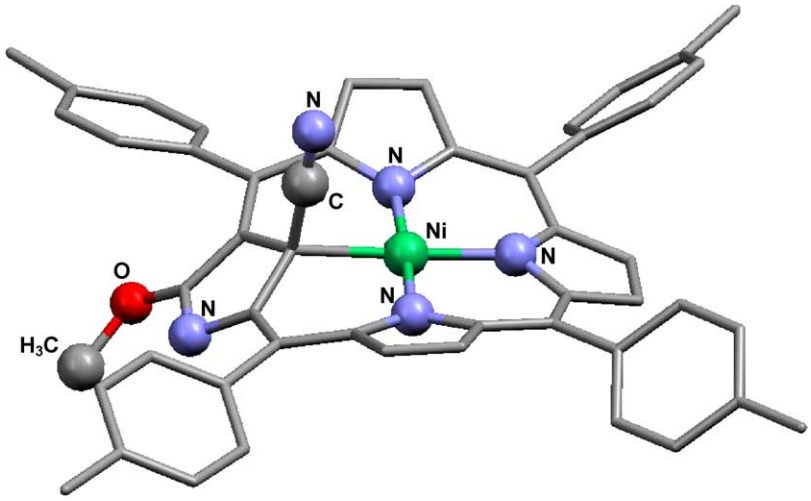

Fig. 13. Crystal structure of Ni((C–CN)(C–OMe)NCTTP) [46].

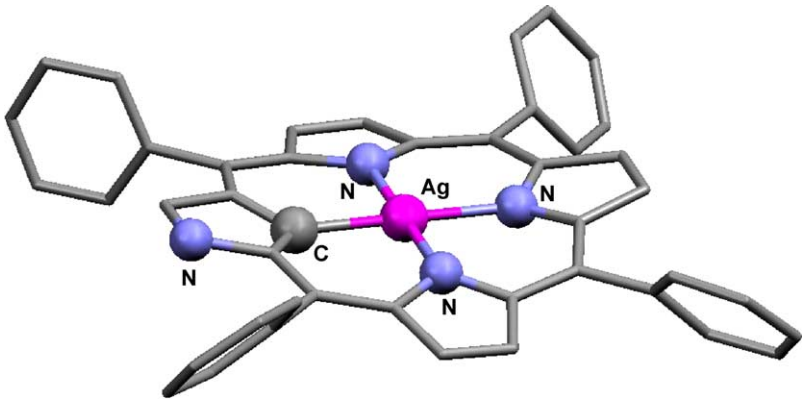

Fig. 14. Crystal structure of Ag(NCTPP) [47]. The external nitrogen is not protonated.

thought to be Cu(NCTPP) with an axial chloride. These same spectra can be obtained by reaction of H_2NCTPP with $CuCl_2$. The product of the metallation reactions were not characterized by X-ray crystallography.

Chmielewski and coworkers also isolated the mono and dimethylated copper species by reaction of mono or dimethyl free base H_2NCTPP with copper chloride in refluxing THF [44]. Extraction of the product with toluene produces the methylated copper adducts with an axial chloride. The EPR and absorption spectra of these products resemble those of the non-methylated Cu(NCTPP)Cl. The dimethylated Cu(2-N$CH_3$21–CCH_3NCTPP) species also could be obtained by reaction of Cu(2-NCH_3NCTPP) with CH_3I in CH_2Cl_2 for 7 days.

Further work on the metallation reaction of N-confused porphyrin with Cu was carried out by Furuta and coworkers [48]. Upon exposure of H_2NCTPP to $Cu(OAc)_2$ under aerobic conditions, the macrocycle is oxidized to form an aryl-substituted tripyrrinone derivative, shown in Scheme 3. The resulting copper tripyrrinone (Fig. 15) can then be substituted with other metals after copper demetallation with sulfuric acid, and the metals Zn(II), Ni(II), Pd(II), Pt(II) and Co(II) were reacted with the tripyrrinone free base. This regioselective ring opening of N-confused porphyrin does not occur if hindering groups were placed at the ortho positions of the meso aryl groups. Furuta and coworkers theorize that electron transfer from copper to molecular oxygen catalyzes ring opening in this reaction. This reaction can proceed in the absence of light, so it does not involve the formation of singlet oxygen as a key step in the ring opening reaction.

The main group element antimony was also incorporated into the core of the macrocycle by stirring H_2NCTTP in dry

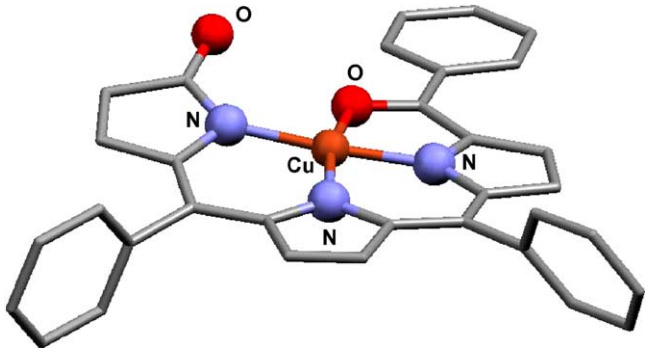

Fig. 15. Crystal structure of Cu tripyranone [48].

$$H_2NCTTP + SbBr_3 \xrightarrow[CH_2Cl_2/MeOH]{\text{dry pyridine}} Sb(NCTTP)(OMe)_2$$

Scheme 4.

pyridine in the presence of a large excess of $SbBr_3$ under nitrogen [49]. Subsequent purification by alumina and silica chromatography with crystallization from CH_2Cl_2/MeOH gives $Sb(NCTPP)(OMe)_2$ (Scheme 4). The structure of the porphyrin ring is planar with a six coordinate antimony lying directly in the center of the core and bent methoxy groups extending from the axial positions (Fig. 16). The ^{1}H NMR data show no interior carbon or exterior nitrogen protons, and the lack of counter anions indicates that NCTPP is acting as a trianion. With the two methoxy groups coordinated to the axial sites above and below the metal, the antimony is clearly in the +5 oxidation state. The absorption spectrum in CH_2Cl_2 displays features very similar to those of the internally protonated tautomer with a red shifted Soret at

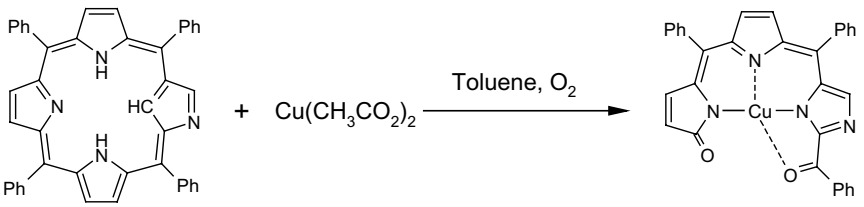

Scheme 3.

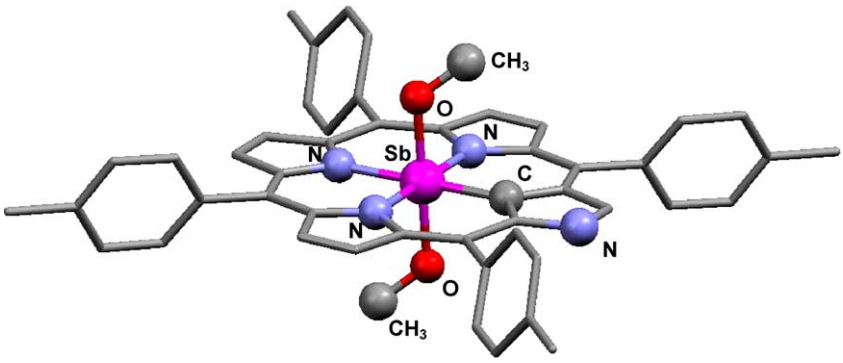

Fig. 16. Crystal structure of Sb(NCTTP)(OCH_3)$_2$; due to disorder resulting from the high symmetry in the structure, the confused pyrrole assignment is ambiguous and 1 of 8 possible orientations is shown [49].

445 nm and three Q-bands at 553, 596, 683 nm, the first two Q-bands being red shifted and the last Q-band being blue shifted relative to the free base.

Chen and Hung isolated the first iron complex of N-confused porphyrins by reacting H_2NCTPP with five equivalents of iron(II) bromide in an anaerobic solution of CH_3CN/THF with a few drops of lutidine [50]. The resultant reaction solution was heated to 65° for 2 h and subsequent concentration of the solution resulted in a crystalline material that was filtered and washed with CH_3CN. The product was vacuum dried and recrystallized from CH_2Cl_2/hexanes under anaerobic conditions. UV–Vis absorption spectroscopy of the product in CH_2Cl_2 shows a large Soret band at 461 nm and a broad Q band at 744 nm. Evan's method of magnetic susceptibility at room temperature gives $\mu_{eff} = 4.85\,\mu_B$ which is similar to that of a high spin d^6 Fe with four unpaired electrons ($\mu_{eff} = 4.90\,\mu_B$).

Single crystal X-ray analysis of the product resulted in the structural elucidation of Fe(NCTPP)Br, shown in Fig. 17 [50]. The structure shows a previously unobserved binding mode for a metal to NCTPP. The most distinguishing characteristic of this species is the presence of a hydrogen on the interior carbon pyrrolic position, resulting in an asymmetric coordination mode for the metal. The iron is a five coordinate distorted square pyramidal complex with the metal 0.50 Å above the nitrogen mean plane. The inverted pyrrole ring is tilted out of the plane of the macrocycle away from the metal center. The bond lengths to the nitrogens adjacent to the confused pyrrole are longer than the bond to the opposite nitrogen. The decrease to the opposite nitrogen results in part from the steric interactions from the proton on the internal carbon. The bond angle between the inverted pyrrole and the Fe(1)–C(1) bond is 126.2° while the angle of the bromide to the internal nitrogen mean plane is 107.0°, leaning toward the inverted pyrrole.

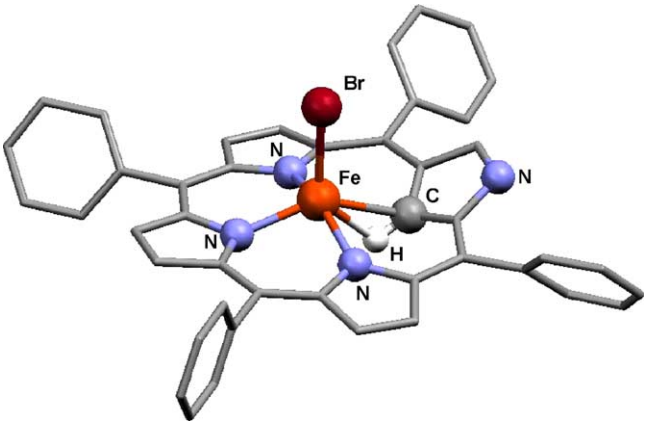

Fig. 17. Crystal structure of Fe(NCTPP)Br [50]. The external nitrogen is protonated.

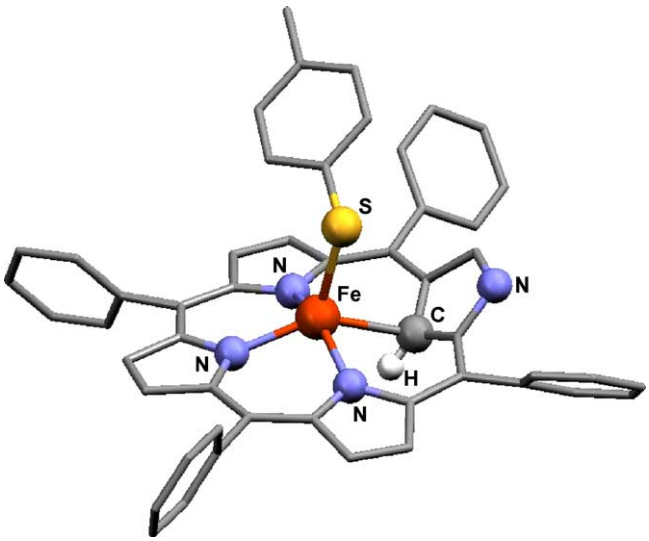

Fig. 18. Crystal structure of Fe(NCTPP)SC_7H_7 [50]. The external nitrogen is protonated.

Fe(NCTPP)Br was then reacted with 4-methylbenzenethiolate ($SC_7H_7^-$) in THF under anaerobic conditions at 65° for 5 h [50]. Upon cooling of the reaction mixture and filtering to remove impurities, a second iron species, Fe(NCTPP)(SC_7H_7), is obtained in 78% yield. Structural characterization by X-ray crystallography was also carried out on this compound after recrystallization from CH_2Cl_2/hexanes. The structure of this species is shown in Fig. 18, and it is very similar to that of the

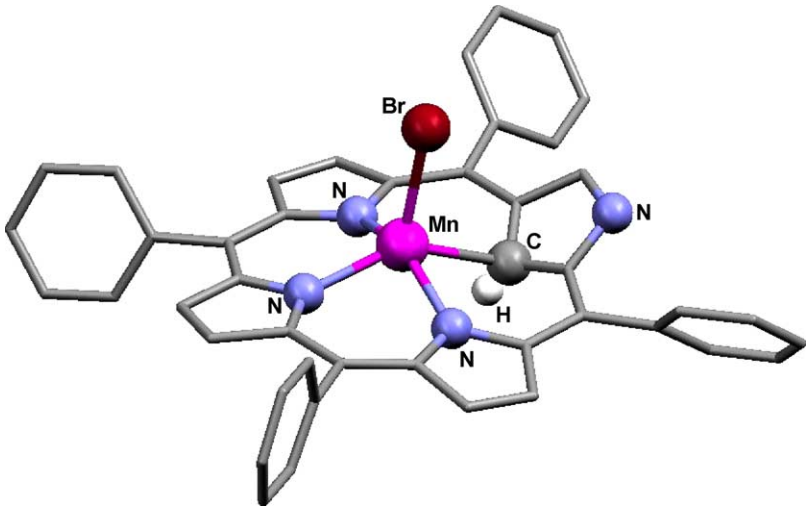

Fig. 19. Crystal structure of Mn^{II}(NCTPP)Br [51]. The external nitrogen is protonated.

bromide compound. The bond lengths exhibit similarities to Fe(NCTPP)Br with the exception of the agostic interaction Fe(1)–H, which is lengthened by 0.334 Å. The tilt of the inverted pyrrole is 116.1°, which is less planar than Fe(NCTPP)Br. The axial thiolate is also tilted more toward the inverted pyrrole with an angle of 118.6° from the nitrogen mean plane. The increase in tilt of the confused pyrrole along with the increase in angle of the axial thiolate ligand forces the metal center to be more tetrahedral in geometry. The magnetic susceptibility of Fe(NCTPP)(SC_7H_7) is $\mu_{eff} = 2.77\,\mu_B$, which is indicative of an intermediate spin system. The UV–Vis absorption of this species is similar to that of Fe(NCTPP)Br with the exception of a 3 nm blue shift of the Q band.

Bohle et al. were also able to incorporate manganese into the core of N-confused porphyrin using manganese(II) bromide following the same metallation procedure for iron, yielding Mn^{II}(NCTPP)Br in 82% yield [51]. The absorption spectrum exhibits a Soret band at 462 nm and two Q bands at 715 and 782 nm. SQUID magnetic susceptibility of 5.50 μ_B, along with an axial ESR spectrum with $g_{||} = 2.01$ and $g_{\perp} = 5.65$, indicate a Mn^{II} metal center with a high-spin $S = 5/2$ spin state. X-ray crystallographic analysis of the product confirms the presence of Mn^{II}(NCTPP)Br (Fig. 19). As in the iron complexes, the confused pyrrole ring is tilted out of the plane of the macrocycle and the manganese atom lies 0.77 Å above the plane of the three internal nitrogens. The manganese bond distance to the nitrogen opposite the confused pyrrole is shorter than the adjacent Mn–N bonds, indicating a possible steric interaction with the internally protonated carbon. The manganese has a five coordinate, distorted square pyramidal geometry. The authors assign a proton to the external pyrrolic position, so that with the axial bromide the metal is assigned the Mn(II) oxidation state, in agreement with the SQUID measurement.

Exposure of Mn^{II}(NCTPP)Br to air in solution causes an immediate change in the visible spectrum [51]. The Soret band of Mn^{II}(NCTPP)Br at 462 nm red shifts to 507 nm with Q band shifts to 754 and 825 nm, respectively. The magnetic susceptibility of the air exposed product is 4.87 μ_B, indicating a Mn^{III} center. The structure of this compound was elucidated by X-ray crystallography, and is shown in Fig. 20. Oxidation of Mn^{II}(NCTPP)Br results in the formation of a metal-deprotonated carbon bond, as seen in the Ni and Ag metallation products. The resultant NCTPP ring is more planar and exhibits identical Mn–N and Mn–C bond distances. The metal is again coordinated by a bromine in the axial position, and with a proton assigned to the external pyrrolic nitrogen, this results in an oxidation state assignment of Mn(III) for the metal center.

At the time of publication of the manganese work by Hung and coworkers, our group presented an alternate synthesis of Mn N-confused porphyrin [52]. Reaction of H_2NCTPP with one metal mole equivalent of $Mn_2(CO)_{10}$ in toluene under anaerobic conditions yields a green product in quantitative yield. Recrystallization from pyridine/heptanes yields large single crystals suitable for X-ray crystallographic structure elucidation. The structure of the product isolated from pyridine, Mn(NCTPP)(py) (Fig. 21) demonstrates

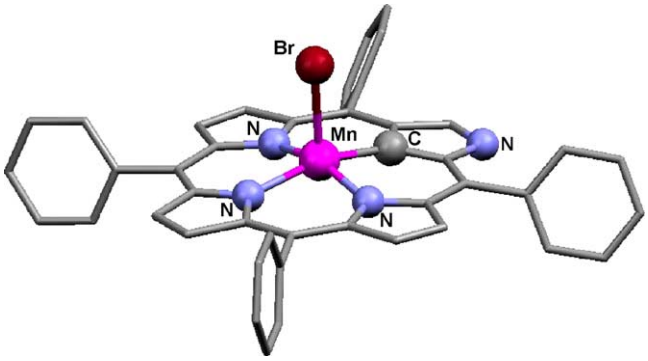

Fig. 20. Crystal structure of Mn^{III}(NCTPP)Br [51]. The external nitrogen is protonated.

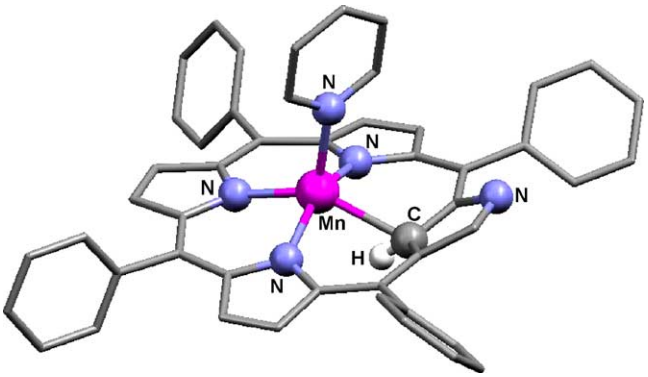

Fig. 21. Crystal structure of Mn(NCTPP)(py) [52]. The external nitrogen is not protonated.

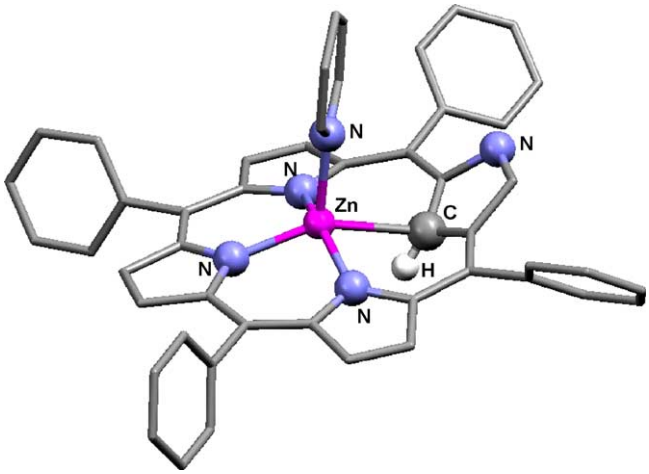

Fig. 22. Crystal structure of Zn(NCTPP)(py) [54]. The external nitrogen is not protonated.

similar structural features to that of Fe^{II}(NCTPP)Br and Mn^{II}(NCTPP)Br. The internal pyrrolic carbon–hydrogen bond is still present and causes similar tilting in the confused pyrrole as that observed in the iron complexes. As seen in Fig. 21, the environment about the metal center Mn(NCTPP)(py) is an asymmetric five coordinate geometry including interactions from the confused pyrrolic carbon. The axial pyridine is disordered with two primary orientations; one is largely orthogonal to the macrocycle plane, similar to the bromide orientation in Fe^{II}(NCTPP)Br, while the other exhibits a tilt analogous to that seen in the axial thiolate in Fe(NCTPP)(SC_7H_7). Unlike the iron complexes, the external proton is absent in this structure due to the absence of anions in the structure. The observed lack of stability of Mn(I) porphyrins is in agreement with this assignment. The N-confused porphyrin ring is clearly dianionic, leading to an oxidation state assignment of Mn(II). As in normal five-coordinate manganese porphyrins, the manganese atom lies 0.509 above the plane of the internal nitrogens and a shorter Mn–N bond to the nitrogen opposite the confused pyrrole is observed [53]. In non-coordinating solvents, such as toluene, this manganese species self coordinates to form a dimer, as will be discussed later. The absorption spectrum of Mn(NCTPP)(py) exhibits a red shifted Soret band at 462 nm and a broad Q band at 691 nm, with a shoulder at 630 nm. Exposure of this complex to air results in shifts in the Soret and Q bands similar to those observed in the work of Hung and coworkers in their Mn(III) species.

The retention of the interior C–H bond in a metal complex was also observed upon metallation of H_2NCTPP with zinc ion, and was first observed by Latos-Grażyński and Chmielewski et al. [44]. Reaction of a H_2NCTPP solution in CH_2Cl_2 with a methanolic solution containing zinc acetate dihydrate and subsequent workup with sodium chloride give Zn(NCTPP)Cl as a green product. NMR experiments show signals in the upfield region at −0.63 ppm, corresponding to the internal pyrrolic CH. Addition of strong base results in disappearance of the proton on the external nitrogen, but the internal proton resonance is still present and shifts to −3.7 ppm.

Explicit structural determination of a monomeric Zn complex was recently completed by Furuta et al. [54]. Reaction of H_2NCTPP and two equivalents of zinc acetate dihydrate in CH_2Cl_2 results in the formation of novel zinc dimers, as will be discussed later. These dimers can be transformed into a monomeric zinc N-confused porphyrin complex bearing an axial pyridine, Zn(NCTPP)(py). Single crystals of the zinc monomer complex suitable for X-ray diffraction were isolated by recrystallization from pyridine/hexanes. In the resultant structure (Fig. 22), the zinc atom lies 0.472 Å above the plane and the confused pyrrole is canted at an angle of 29.2° relative to the plane of the ring. The internal and external protons are assigned, resulting in a dianionic charge for the macrocycle. The absorption spectrum shows similarities to the externally protonated free base tautomer with a red shifted Soret band at 467 nm and Q-bands at 591, 635, and 704 nm, respectively.

Furuta et al. also isolated a second monomeric Zn(NCTPP) with an axial coordinating isopropanol by recrystallization of a zinc dimer complex from CH_2Cl_2/isopropanol [55]. Retention of the internal CH was observed at −3.68 ppm in NMR experiments. The structure of this compound was elucidated by X-ray crystallography, and is shown in Fig. 23. As in the pyridine adduct, the zinc atom is five coordinate with the zinc atom lying 0.45 Å above the plane and the confused pyrrole is tilted at an angle of 28.9 in relation to the 24 core atoms.

Very recently, Furuta and coworkers synthesized N-confused pentafluorophenylporphyrin (H_2NCTPFPP) by a [2 + 2] condensation route [56]. The absorption spectrum of the free base is blue shifted compared to H_2NCTPP, with a Soret band at 434.5 nm and Q bands at 528, 568, and 712 nm. This electron withdrawing porphyrin unit was subsequently reacted with Ag, Cu, Pd, and Ni salts. All metal complexes formed were square planar, similar to those observed for Ni(NCTPP). Unlike H_2NCTPP, H_2NCTPFPP copper derivative crystals were isolated and the X-ray structure

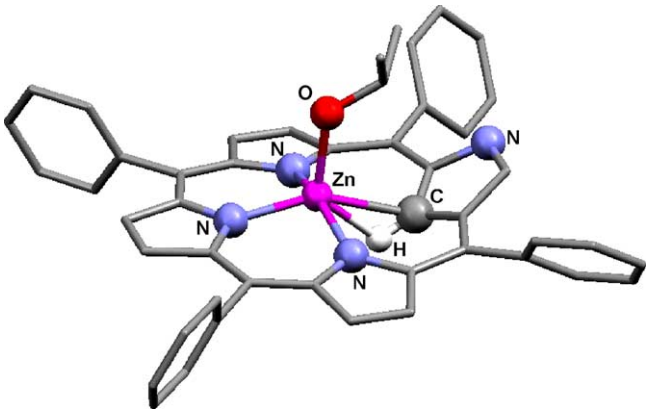

Fig. 23. Crystal structure of Zn(NCTPP)(isopropanol) [55].

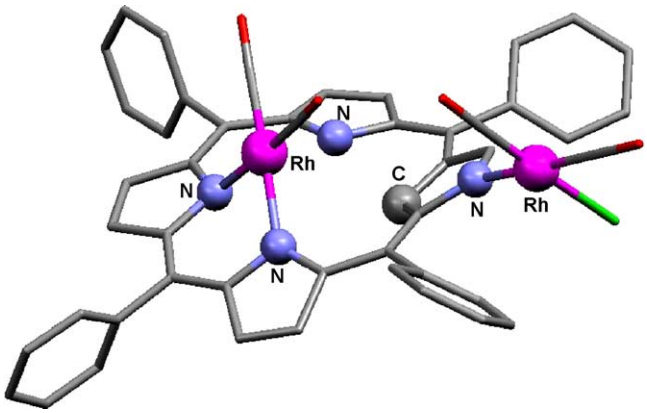

Fig. 25. Crystal structure of Rh_2(NCTPP) [64].

is shown in Fig. 24. As seen before for the internally deprotonated metal complexes with NCTPP, NCTPFPP in Ag(NCTPFPP) is acting as a trianion while acting as a dianion for the Ni, Pd, and Cu NCTPFPP complexes.

2.2. Dimeric complexes

In normal porphyrins, the geometry of metal binding is typically limited to monomeric forms where the metal resides close to or within the plane of the macrocycle [2]. However, in certain circumstances dimeric complexes can form. This is observed for large metal ions which do not fit well in the pore of the macrocycle, as in $Zr(TPP)_2$ and $U(TPP)_2$ [57–60]. Alternatively, there are many examples where metal–metal bond formation promotes dimerization, as seen in $[Rh(TPP)]_2$ and $[Ru(TPP)]_2$ [61–63]. In N-confused porphyrins, the asymmetric nature of the macrocycle ring leads to a larger diversity of binding modes, and a number of novel dimeric metal complexes have been observed, frequently involving coordination by the confused pyrrole ring.

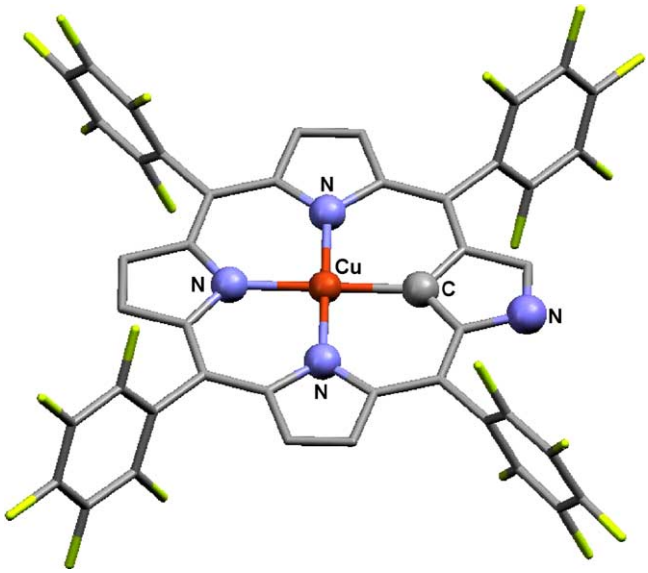

Fig. 24. Crystal structure of Cu(NCTPFPP); due to disorder resulting from the high symmetry in the structure, the confused pyrrole assignment is ambiguous and one of eight possible orientations is shown [56].

Since the confused pyrrole in H_2NCTPP contains an external nitrogen, it was believed that this site could also engage in metal binding. The binding of this nitrogen to a metal center was observed by Furuta and co-workers who isolated a rhodium NCTPP adduct that exhibited both interior and exterior coordination to two rhodium ions (Fig. 25) [64]. Furuta and co-workers synthesized this complex by reacting H_2NCTPP with one equivalent of $[Rh(CO)_2Cl]_2$ in the presence of 10 equivalents of sodium acetate in refluxing CH_2Cl_2 for 2 h. As seen in the figure, the X-ray crystal structure shows that one rhodium center is coordinated to the external nitrogen and the second rhodium is coordinated to two nitrogens, one imino (N3) and one amino (N4), on the interior of the macrocycle. Both rhodium ions are located above the plane of the macrocycle and exhibit square planar geometries. The UV–Vis absorption spectrum of this complex displays a 50 nm red shifted Soret band at 488 nm with four less intense red shifted Q bands ranging from 545 to 780 nm.

In a separate study, Furuta et al. experimented with solvent conditions to see its effect on metal coordination of palladium to H_2NCTTP [65]. The reaction of $Pd(OAc)_2$ with H_2NCTTP in $CHCl_3$ yields the internally metallated form in 50% yield. X-ray crystallographic analysis (Fig. 26) shows that the Pd is in the plane of the macrocycle and the internal carbon is coordinated to the metal, supporting ^{1}H NMR data of the absence of the internal and external protons. This structure is directly analogous to that of the nickel compound. The absorption spectrum shows a Soret at 416 nm along with Q-bands at 534, 577, 643, 700, and 766 nm.

However, if the solvent for metallation is changed to toluene, two dimer species along with the internally metallated monomer can form [65]. Purification by silica gel yields the dimers and monomer in 27, 36, and 19%, respectively (Scheme 5). The dimers are made up of two NCTTP units and two metals. As seen in Fig. 27, the external nitrogen

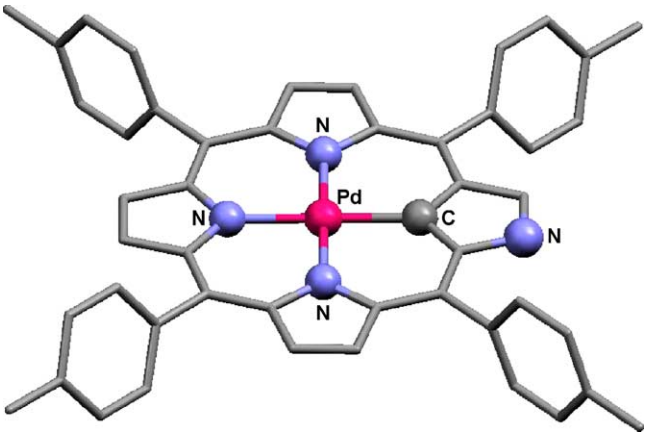

Fig. 26. Crystal structure of Pd(NCTTP); due to disorder resulting from the high symmetry in the structure, the confused pyrrole assignment is ambiguous and one of eight possible orientations is shown [65].

and an ortho carbon from the tolyl group of one macrocycle and two internal nitrogens from the second macrocycle coordinate to each palladium. The two Pd metal sites in this compound are quite different, with one site being nearly square planar and the second metal site being tetrahedral. The only differences between the dimers are the orientations of the coordinating NCTTP units. In one structure, the internal protons on each NCTTP plane are oriented in the same direction, while the other dimer is believed to have the internal proton on each macrocycle opposite to each other. The absorption spectra for the dimers are similar in structure, with the Soret band being red shifted to 470 nm and Q bands ranging from 600 to 835 nm.

While investigating the flexible inner and outer coordination chemistry of N-confused porphyrin, Furuta et al. synthesized two dimers incorporating zinc ions [54]. H_2NCTPP was reacted with two equivalents of zinc acetate dihydrate in CH_2Cl_2 at room temperature. Removal of the solvent and crystallization from toluene/hexanes gives a dimer complex containing four zinc atoms (Fig. 28). This form is unique because the external nitrogen is coordinated to a bridging dizinc acetate unit with the acetate oxygens occupying the axial positions of the zinc NCTPP macrocycles. The geometries about bridging zinc atoms are tetrahedral while the zinc sites in the NCTPP core are roughly pentacoordinate.

The bridging zinc molecules could be removed by addition of 1% $(Et_4N)OH$ in aqueous solution [54]. After removal of the bridge, characterization by ^{1}H NMR and ^{15}N NMR of this compound in CH_2Cl_2 led Furuta to propose that the Zn(NCTPP) units were forming dimers without the bridging dizinc unit, with the external nitrogen coordinating the axial position of the second macrocycle. Reaction of the Zn(NCTPP) dimer with pyridine led to the formation of monomeric Zn(NCTPP) with an axial pyridine, as previously described. The UV-Vis absorption spectra of the three zinc species exhibit many similarities, with only minor shifts

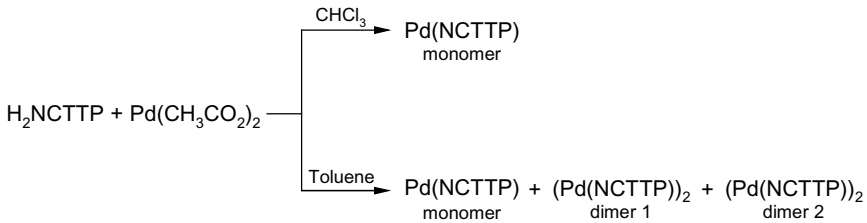

Scheme 5.

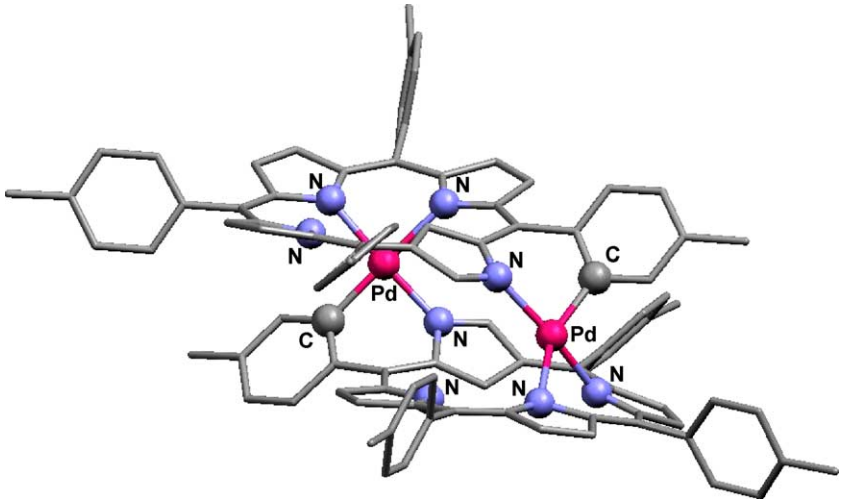

Fig. 27. Crystal structure of $[Pd(NCTTP)]_2$ [65].

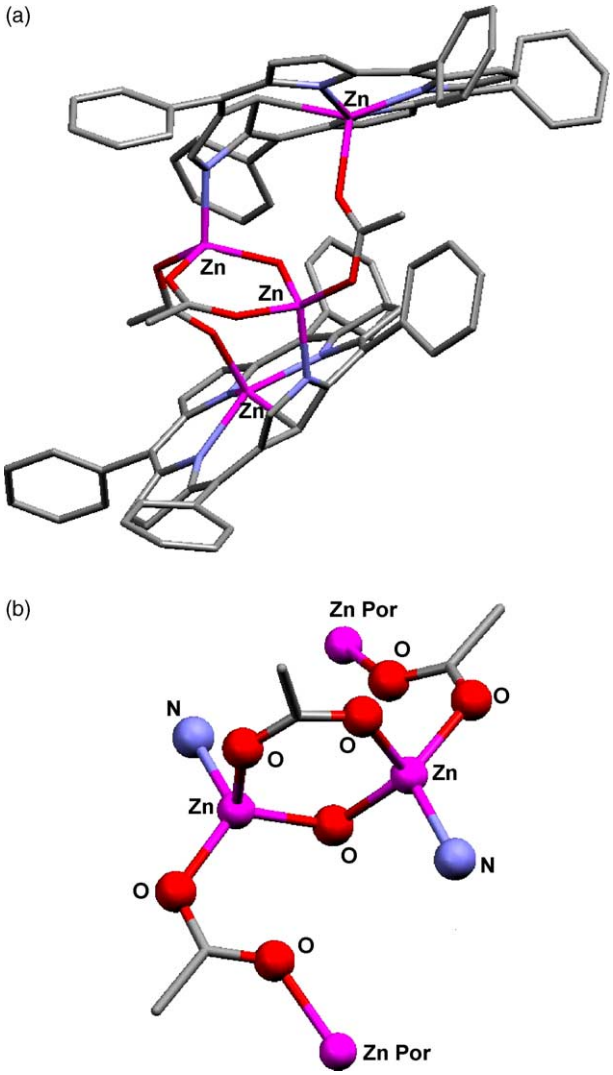

Fig. 28. Crystal structure of Zn_4 NCTPP dimer (a), with a close up of the bridging diacetate unit (b) [54].

in the Soret and Q-bands. The confused pyrrole ring is tilted from the plane at an angle of 36.1 and 29.2° for monomer and dimer, respectively, as seen in both Fe(NCTPP) monomer complexes.

Similar dimer chemistry was also observed in the iron and manganese metallation reactions [52,66]. Hung and Chen continued their investigation of Fe(NCTPP)Br by reacting this molecule with NaSePh in THF. Isolation of the product yielded a dark green crystalline material in 85% yield. The absorption spectrum of the product displays a Soret band at 459 nm and broad Q bands structures at 755 nm with a shoulder at 660 nm. SQUID magnetic susceptibility measurements of the compound provides a magnetic moment of 4.31 μ_B at 300 K and 1.64 μ_B at 6 K, however, the authors do not have enough data to support antiferromagnetic coupling in the product.

X-ray crystallographic analysis of the product of this reaction with NaSePh in THF revealed a new coordination

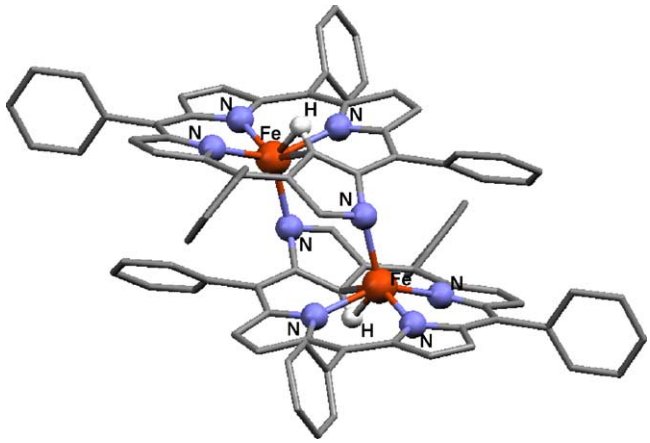

Fig. 29. Crystal structure of $[Fe(NCTPP)]_2$ [66].

mode of N-confused porphyrin (Fig. 29) [66]. As was suggested by Furuta's NMR experiments on Zn(NCTPP), metal adducts of N-confused porphyrins have the ability to form self-coordinating dimers in the absence of strong coordinating ligands. The interior C–H bond is still intact and a similar tilting is observed for the confused pyrrole. One of the phenyl rings of each coordinating unit rotates 44.6° to relieve steric interactions. The coordination geometry about the iron centers is similar to that observed in Fe(NCTPP)Br. With the exception of the axial coordination, similar Fe–N bond distances are observed and the agostic interaction with the internal CH is still present. The axial site of the iron is occupied by the external nitrogen of the second Fe(NCTPP) ring.

In solution, this adduct is very sensitive to molecular oxygen. Upon exposure of $[Fe(NCTPP)]_2$ in THF to molecular oxygen, a rapid shift and broadening in the Soret band from 455 to 389 nm with no observable Q band region [66]. The structure of this iron complex shows a new conformation for the porphyrin rings (Fig. 30). As in normal oxidation of iron(II) porphyrins, a bridging oxygen links the two iron centers of the dimer. Unlike normal porphyrins, the Fe–O–Fe bond angle is bent, suggesting a μ-hydroxo bridge. In addition to the bridging hydroxo, oxygenation of the confused

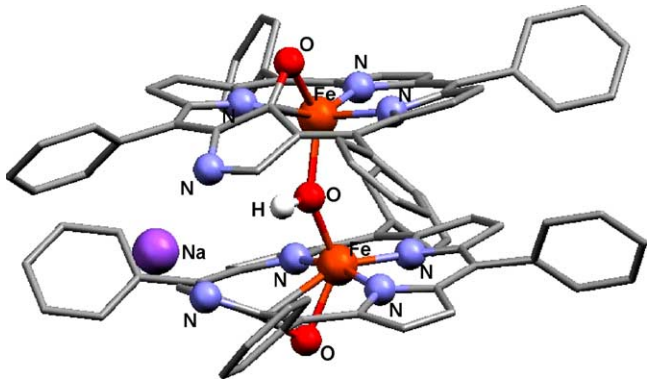

Fig. 30. Crystal structure of $[Fe(ONCTPP)]_2OH{\cdot}Na(THF)_2$ [66].

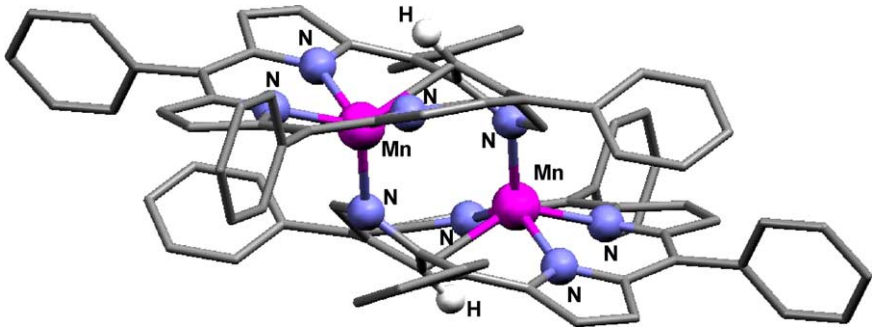

Fig. 31. Crystal structure of [Mn(NCTPP)]$_2$ [52].

pyrrolic hydrogen has taken place, generating an internal N-confused porphyrin oxo adduct. A sodium atom also coordinates to the external nitrogens of each confused ring.

In our reaction of $Mn_2(CO)_{10}$ with H_2NCTPP, a broad absorption band was observed in the Soret region, a distinctly different spectrum from that of the free base precursor [52]. The Soret band at 413 nm is broad and has a low extinction coefficient of 5.16×10^4 M^{-1} cm^{-1}. In addition, a Q band at 683 nm with a shoulder at 625 nm is observed. Unlike the manganese adduct presented by Hung and coworkers, this Mn(NCTPP) species is extremely air sensitive, rapidly demetallating to the free base upon exposure to atmospheric dioxygen. A green product was isolated upon recrystallization from the non-coordinating solvents toluene/heptanes in 73% yield.

Elucidation of the structure of this species by X-ray crystallography was completed using crystals obtained from hot toluene [52]. The elucidated structure reveals that this complex forms a dimer in the solid state. The structure observed in this Mn dimer is directly analogous to that seen in the Fe dimer system prior to oxidation. As can be seen in Fig. 31, this species is a self-coordinated manganese N-confused porphyrin, where the external nitrogen of one macrocycle is ligated to the axial position in the second. The proton on the interior carbon is still present, and the confused pyrrole ring is tilted away from the metal. The resultant deformation of the macrocycle ring is significant: the confused pyrroles are at an average angle of 44.0° from the plane of the three internal nitrogen atoms and four of the phenyl rings per dimer are nearly coplanar (average angle 34.0°) with the porphine ring. Within the two dimers, the manganese atoms are an average of 5.06 Å apart and the porphine rings are 4.32 Å away from each other, using the planes of the inner pyrrolic nitrogens. As in the bromide or pyridine forms, the metal is five-coordinate and extends above the plane of the three internal nitrogens by 0.757 Å.

In more recent work, metallated N-confused porphyrins have been linked into dimers using covalent bonds at the external nitrogen [67,68]. Chmielewski and Schmidt continued their work with Ni(NCTPP) by examining the reactions with CH_2Br_2 or CH_2I_2. Purification of the products by chromatography affords two bands, and characterization of these two products by NMR provides information on the probable stacking orientations of the NCTPP units in the dimer. Two dimers are obtained from the reaction, the major component of which is two Ni(NCTPP) units bound together through a methyl linker at the 2 and 21′ position of each macrocycle (internal to external). The second dimer is made up of two Ni(NCTPP) units bridged by a methyl linker through the external nitrogens. The absorption spectrum of the internal to externally bridged unit displays a Soret band at 431 nm with a shoulder at 465 nm and broad Q bands. The externally bridged complex exhibits similar characteristics, but the Soret is split (429 and 468 nm) and less intense.

Reaction of sodium ethoxide with Ni(NCTPP) in CH_2Cl_2 under anaerobic conditions results in the addition of a methoxy ethyl group at the internal carbon, with a second minor product having methoxy ethyl at the external nitrogen [68]. If the reaction is done in the presence of K_2CO_3/dibenzo[18]-crown-6, the externally coordinated form is favored. The absorption spectra of Ni(21-ethoxymethyl NCTPP) is similar to the internally methylated derivative with a Soret at 429 nm and an undefined Q band structure, while the Ni(2N-ethoxymethyl NCTPP) is similar to the externally methylated form (Soret at 427 and 460 nm, Q bands at 533, 560, 593, 649, 720 and 789 nm). ^{1}H NMR of Ni(21-ethoxymethyl NCTPP) shows signals at −1.29 and −1.38 ppm, correlating to inequivalent methylene protons from the methyl linker.

Chmielewski and Schmidt also reacted Ni(NCTPP) with 1,2-dibromoethane and formed the 21,21′ ethylene linked Ni(NCTPP) dimer, with Ni(2N-bromoethane NCTPP) being a byproduct [68]. No 2,2′ ethylene linked porphyrin was observed in the reaction mixture. The NMR of this dimer species gives rise to three possible isomers, depending on the orientation of the confused pyrrolic nitrogen. The external nitrogens could be stacked in the same orientation or staggered if one macrocycle is flipped upon another. Ni(2N-bromoethane NCTPP) has absorption characteristics similar to Ni(NCTPP) and the externally coordinated derivatives. Structural elucidation of this complex was completed by X-ray crystallography (Fig. 32). The nickel ion is essentially in the plane of the internal nitrogens, while the confused pyrrole is tilted from the plane and the macrocycle

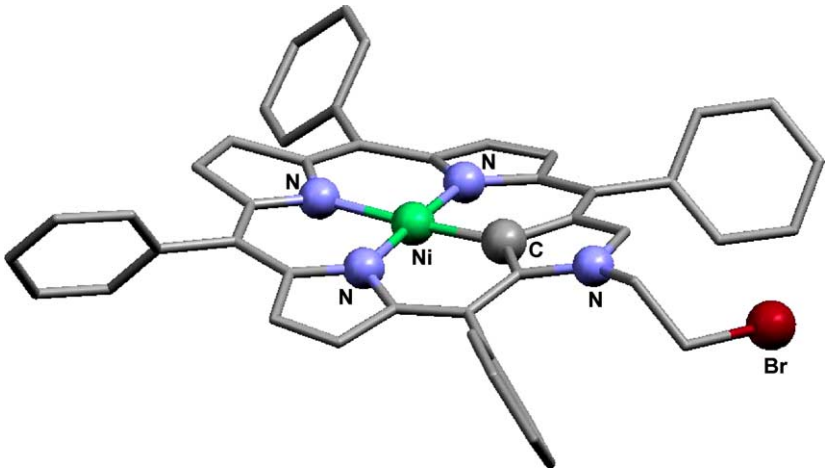

Fig. 32. Crystal structure of Ni(N2-bromoethyl-NCTPP) [68].

adopts a saddle like structure. Lastly, reaction of Ni(NCTPP) with 1,3-dibromopropane in THF with *tert*-BuOH results in the formation the monomeric Ni(21-propylene NCTPP), where internal substitution of a propylene group at the internal CH is observed in the NMR spectrum.

Following analogous metallation procedures for the formation of Pd(NCTPP) dimer complexes, Furuta and coworkers were able to generate platinum(II) monomer and dimer complexes with 5,10,15,20-tetrakis(4′-*tert*-butylphenyl)-porphyrin ($NCT_{4't-Bu}PP$) in refluxing toluene with 0.5 equivalent $PtCl_2$ [69]. As seen in the Pd complexes, ortho carbon activation of one of the aryl rings is also seen in the Pt complexes, and two geometric isomers are obtained. As seen in Figs. 33 and 34, the Pt in both dimer complexes is bound to the external nitrogens on both porphyrin units, an ortho carbon from one aryl ring, and a chloride. Platinum is in a square planar geometry in both complexes, and the only difference in structure between the two isomers is whether the N-confused porphyrin units are bound *cis* or *trans* to the metal. The absorption spectra of both complexes are very similar, with the *cis* complex having a Soret band at 447 nm and Q-bands at 563, 607, and 785 nm while the *trans* complex has a red shifted Soret at 458 nm and two Q band at 559 and 791 nm. If one equivalent of $PtCl_2$ is used in the reaction, a bis-platinum dimer complex is believed to form with a Pt_2Cl_2 core linking the two N-confused porphyrin units. In both reactions, the monomeric platinum complex with Pt binding in the core of $NCT_{4't-Bu}PP$ is produced as a minor product. Isolation of the molecular structure of the interior metallated product was obtained using 3,5-ditertbutylphenyl N-confused porphyrin.

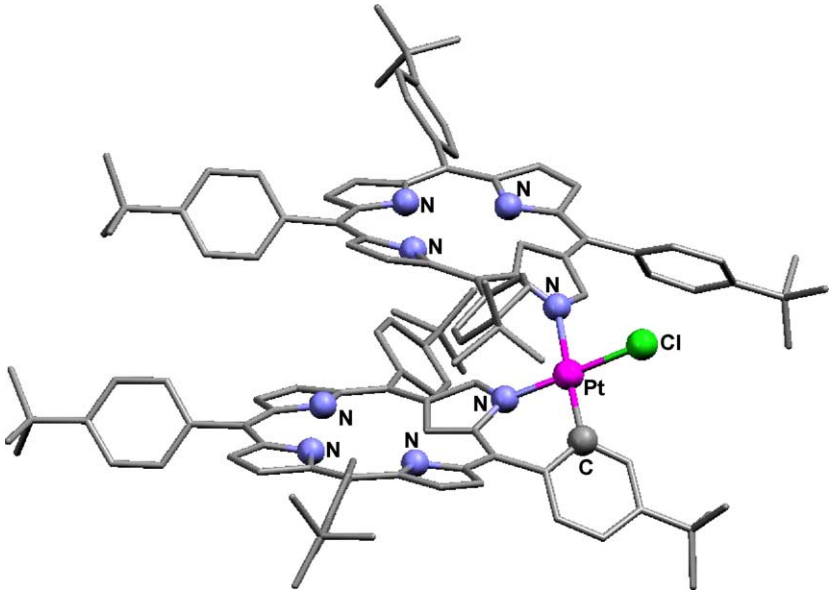

Fig. 33. Crystal structure of *cis*-Pt(NCTTP)$_2$Cl [69].

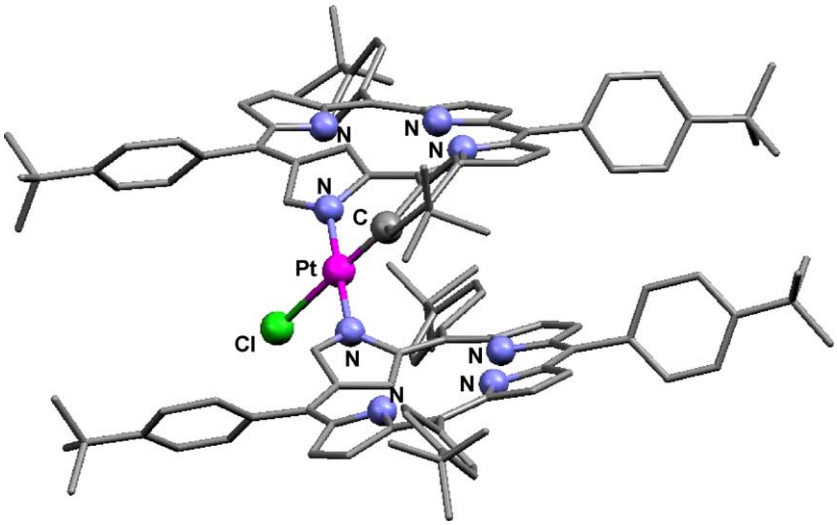

Fig. 34. Crystal structure of *trans*-Pt(NCTTP)$_2$Cl [69].

3. Summary and conclusion

The metal chemistry of N-confused porphyrins has been investigated since the discovery of the macrocycle with the presentation of the nickel complex by Latos-Grażyński [29]. With the recent synthetic advancements of Lindsey and Geier, N-confused porphyrin is now readily available in gram scale quantities to research groups across the globe [31]. This has resulted in an explosion in investigations and publications into the metal chemistry of N-confused porphyrin. Although the metal chemistry of this macrocycle is only beginning to be understood, to date the complexes that have been isolated exhibit a remarkable diversity of both monomeric and dimeric structures.

The metal chemistry of this macrocycle will undoubtedly grow significantly over the next few years. Future investigations should also expand upon this synthetic work to explore the effects of metal binding on the electronic structure of the macrocycle. New N-confused metalloporphyrins can be characterized by using the four orbital model convention developed for metalloporphyrins by Goutermann [38,39]. In addition to examining the electronic structure of the ring system, EPR and Mössbauer investigations can add insight into the nature of metal binding, especially in the cases where the internal C–H bond is retained [50–52,66]. Lastly, the reactivity of N-confused metalloporphyrins should be probed, as is being done with metallocorroles [70]. Such investigations should shed light on the nature of porphyrin catalysis and may provide the opportunity to isolate high valent compounds relevant to the highly oxidizing ferryl intermediates present in heme protein oxidations [71].

References

[1] K.M. Kadish, K.M. Smith, R. Guilard (Eds.), The Porphyrin Handbook, vol. 1–10, Academic Press, New York, 2000.
[2] J.W. Buchler, in: D. Dolphin (Ed.), The Porphyrins, vol. 1, Academic Press, New York, 1979, p. 389.
[3] T.L. Poulos, in: K.M. Kadish, K.M. Smith, R. Guilard (Eds.), The Porphyrin Handbook, vol. 4, Academic Press, New York, 2000, p. 189.
[4] B. Meunier, A. Robert, G. Pratviel, J. Bernadou, in: K.M. Kadish, K.M. Smith, R. Guilard (Eds.), The Porphyrin Handbook, vol. 4, Academic Press, New York, 2000, p. 119.
[5] K.M. Kadish, K.M. Smith, R. Guilard (Eds.), The Porphyrin Handbook, vol. 6, Academic Press, New York, 2000.
[6] J. Wojaczynski, L. Latos-Grażyński, Coord. Chem. Rev. 204 (2000) 113.
[7] H. Fujii, Coord. Chem. Rev. 226 (2002) 51.
[8] K. Nakamoto, Coord. Chem. Rev. 226 (2002) 153.
[9] J.L. Sessler, J. Porphy. Phthalocyanines 4 (2000) 331.
[10] H. Furuta, H. Maeda, A. Osuka, Chem. Commun. (2002) 1795.
[11] C.J. Fowler, J.L. Sessler, V.M. Lynch, J. Waluk, A. Gebauer, J. Lex, A. Heger, F. Zuniga-y-Rivero, E. Vogel, Chem. Eur. J. 8 (2002) 3485.
[12] J. Bendix, I.J. Dmochowski, H.B. Gray, A. Mahammed, L. Simkhovich, Z. Gross, Angew. Chem. Int. Ed. 39 (2000) 4048.
[13] Z. Gross, G. Golubkov, L. Simkhovich, Angew. Chem. Int. Ed. 39 (2000) 4045.
[14] L. Simkhovich, A. Mahammed, I. Goldberg, Z. Gross, Chem. Eur. J. 7 (2001) 1041.
[15] M. Broring, C. Hell, Chem. Commun. (2001) 2336.
[16] D.T. Gryko, K.E. Piechora, J. Porphy. Phthalocyanines 6 (2002) 81.
[17] R. Guilard, D.T. Gryko, G. Canard, J.M. Barbe, B. Koszarna, S. Brandes, M. Tasior, Org. Lett. 4 (2002) 4491.
[18] D.T. Gryko, Eur. J. Org. Chem. (2002) 1735.
[19] B.S. Mandimutsira, B. Ramdhanie, R.C. Todd, H. Wang, A.A. Zareba, R.S. Czernuszewicz, D.P. Goldberg, J. Am. Chem. Soc. 124 (2002) 15170.
[20] A. Jasat, D. Dolphin, Chem. Rev. 97 (1997) 2267.
[21] L. Latos-Grażyński, P.J. Chmielewski, New J. Chem. 21 (1997) 691.
[22] A. Gebauer, J.A.R. Schmidt, J. Arnold, Inorg. Chem. 39 (2000) 3424.
[23] C.-H. Hung, C.-K. Ou, G.-H. Lee, S.-M. Peng, Inorg. Chem. 40 (2001) 6845.
[24] J.-Y. Tung, B.-C. Liau, S. Elango, J.-H. Chen, H.-Y. Hsieh, F-L. Liao, S.-L. Wang, L.-P. Hwang, Inorg. Chem. Commun. 5 (2002) 150.
[25] P.J. Chmielewski, L. Latos-Grażyński, M.M. Olmstead, A.L. Balch, Chem. Eur. J. 8 (1997) 268.
[26] H. Ali, J.E. van Lier, Tetrahedron Lett. 38 (1997) 8173.
[27] M. Pawlicki, L. Latos-Grażyński, Inorg. Chem. 41 (2002) 5866.
[28] H. Furuta, T. Asano, T. Ogawa, J. Am. Chem. Soc. 116 (1994) 767.

[29] P.J. Chmielewski, L. Latos-Grażyński, K. Rachlewicz, T. Glowiak, Angew. Chem. Int. Ed. 33 (1994) 779.
[30] H. Furuta, H. Maeda, A. Osuka, J. Am. Chem. Soc. 122 (2000) 803.
[31] G.R. Geier III, D.M. Haynes, J.S. Lindsey, Org. Lett. 1 (1999) 1455.
[32] G.R. Geier III, Y. Ciringh, F. Li, D.M. Haynes, J.S. Lindsey, Org. Lett. 2 (2000) 1745.
[33] L. Szterenberg, L. Latos-Grażyński, Inorg. Chem. 36 (1997) 6287.
[34] A. Ghosh, T. Wondimagegn, H.J. Nilsen, J. Phys. Chem. B 102 (1998) 10459.
[35] H. Furuta, H. Maeda, A. Osuka, J. Org. Chem. 66 (2001) 8563.
[36] H. Furuta, T. Ishizuka, A. Osuka, H. Dejima, H. Nakagawa, Y. Ishikawa, J. Am. Chem. Soc. 123 (2001) 6207.
[37] J.P. Belair, C.J. Ziegler, C.S. Rajesh, D.A. Modarelli, J. Phys. Chem. A 106 (2002) 6445.
[38] M.J. Gouterman, in: D. Dolphin (Ed.), The Porphyrins, vol. III, Academic Press, New York, 1978, pp. 1–165.
[39] P.G. Seybold, M.J. Gouterman, J. Mol. Spectrosc. 31 (1969) 1.
[40] L. Simkhovich, I. Goldberg, Z. Gross, Inorg. Chem. 41 (2002) 5433.
[41] A. Antipas, M. Gouterman, J. Am. Chem. Soc. 105 (1983) 4896.
[42] P.J. Chmielewski, L. Latos-Grażyński, T. Głowiak, J. Am. Chem. Soc. 118 (1996) 5690.
[43] P.J. Chmielewski, L. Latos-Grażyński, J. Chem. Soc. Perkin Trans. 2 (1995) 503.
[44] P.J. Chmielewski, L. Latos-Grażyński, I. Schmidt, Inorg. Chem. 39 (2000) 5475.
[45] Z. Xiao, B.O. Patrick, D. Dolphin, Chem. Commun. (2002) 1816.
[46] Z. Xiao, B.O. Patrick, D. Dolphin, Chem. Commun. (2003) 1062.
[47] H. Furuta, T. Ogawa, Y. Uwatoko, K. Araki, Inorg. Chem. 38 (1999) 2676.
[48] H. Furuta, H. Maeda, A. Osuka, Org. Lett. 4 (2002) 181.
[49] T. Ogawa, H. Furuta, M. Takahashi, A. Morino, H. Uno, J. Organomet. Chem. 611 (2000) 551.
[50] W.-C. Chen, C.-H. Hung, Inorg. Chem. 40 (2001) 5070.
[51] D.S. Bohle, W.-C. Chen, C.-H. Hung, Inorg. Chem. 41 (2002) 3334.
[52] J.D. Harvey, C.J. Ziegler, Chem. Commun. (2002) 1942.
[53] B. Gonzalez, J. Kouba, S. Yee, C.A. Reed, J.F. Kirner, W.R. Scheidt, J. Am. Chem. Soc. 97 (1975) 3247.
[54] H. Furuta, T. Ishizuka, A. Osuka, J. Am. Chem. Soc. 124 (2002) 5622.
[55] H. Furuta, T. Ishizuka, A. Osuka, Inorg. Chem. Commun. 6 (2003) 398.
[56] H. Maeda, A. Osuka, Y. Ishikawa, I. Aritome, Y. Hisaeda, H. Furuta, Org. Lett. 5 (2003) 1293.
[57] G.S. Girolami, C.L. Hein, K.S. Suslick, Angew. Chem. Int. Ed. 35 (1996) 1223.
[58] J.W. Buchler, G. Heinz, Chem. Berichte 129 (1996) 201.
[59] J.P. Collman, J.L. Kendall, J.L. Chen, K.A. Collins, J.C. Marchon, Inorg. Chem. 39 (2000) 1661.
[60] G.S. Girolami, P.A. Gorlin, S.N. Milam, K.S. Suslick, S.R. Wilson, J. Coord. Chem. 32 (1994) 173.
[61] S. Lee, M. Mediati, B. Wayland, J. Chem. Soc. Chem. Commun. (1994) 2299.
[62] J.P. Collman, S.T. Harford, Inorg. Chem. 37 (1998) 4152.
[63] K. Funatsu, T. Imamura, A. Ichimura, Y. Sasaki, Inorg. Chem. 37 (1998) 4986.
[64] A. Srinivasan, H. Furuta, A. Osuka, Chem. Commun. (2001) 1666.
[65] H. Furuta, N. Kubo, H. Maeda, T. Ishizuka, A. Osuka, H. Nanami, T. Ogawa, Inorg. Chem. 39 (2000) 5424.
[66] C.-H. Hung, W.-C. Chen, G.-H. Lee, S.-M. Peng, Chem. Commun. (2002) 1516.
[67] I. Schmidt, P.J. Chmielewski, Chem. Commun. (2002) 92.
[68] I. Schmidt, P.J. Chmielewski, Z. Ciunik, J. Org. Chem. 67 (2002) 8917.
[69] H. Furuta, K. Youfu, H. Maeda, A. Osuka, Angew. Chem. Int. Ed. 42 (2003) 2186.
[70] Z. Gross, G. Golubkov, L. Simkhovich, Angew. Chem. Int. Ed. 39 (2000) 4045.
[71] Y. Watanabe, in: K.M. Kadish, K.M. Smith, R. Guilard (Eds.), The Porphyrin Handbook, vol. 4, Academic Press, New York, 2000, p. 97.